

## Transient stability enhancement of virtual synchronous generators with virtual resistance

Emmanuel Ebinyu<sup>1</sup>, Omar Abdel-Rahim<sup>1,2</sup>, Sobhy M. Abdelkader<sup>1,3</sup>,  
Masahito Shoyama<sup>4</sup>, Diao-Eldin A. Mansour<sup>1,5\*</sup>

Virtual synchronous generators (VSGs) incorporate virtual resistance (VR) in inverter control as a damping mechanism for oscillations that appear around the synchronous frequency due to interactions between the inverter impedance and the line impedance while operating in low inertia grids. Damping is critical for synchronization stability in the small-signal and large-signal disturbance scenarios to suppress oscillations that threaten system stability. While VR enhances stability in the steady state, it is shown that its conventional application affects the transient stability of VSGs by reducing the angle overshoot range in the dynamic behaviour of the power angle  $\delta$ , illustrated using the power-angle ( $P - \delta$ ) and frequency-angle ( $\dot{\delta} - \delta$ ) curves. In this article, a novel damping mechanism to improve the transient stability of VSGs using VR to enhance the power angle dynamics is proposed. By using the concept of virtual point of common coupling, the virtual power of the internal VSG is introduced in the active power feedback during a voltage sag, providing an equivalent damping effect proportional to the VR applied. In this way, the negative effects of VR on transient stability are averted while VR is used to improve the power angle dynamics of conventional VSG. Simulations of different transient stability scenarios are carried out in MATLAB/Simulink to verify the proposed method.

Keywords: virtual resistance, virtual power, transient stability, oscillation suppression, virtual synchronous generator, damping

### 1 Introduction

With the proliferation of renewable energy resources into the electric power grid, electronic converters are becoming the dominant power interface devices for energy sources in the grid resulting in the gradual loss of rotational mechanical actuation provided by the synchronous generators (SGs) and a low-inertia paradigm [1]. These low-inertia systems face a range of issues including loss of robust rotational synchronisation, heightened difficulty in voltage and frequency control, and proneness to fault severity owing to the loss of stored energy [2]. Moreover, the fast-actuating power electronics digital controllers introduce a new dynamic scenario that deviates from slow rotating machine-oriented network set-ups of conventional power grids. Consequently, the design of inverters has veered towards conventional grid-friendly designs, which incorporate SG characteristics. To this end, the grid-forming (GFM) control of voltage source converters (VSCs) is being adopted as the preferred control paradigm of grid-interfacing converters [3].

The virtual synchronous generator (VSG) is, therefore, a natural choice for low-inertia systems to tackle frequency and voltage disparities by the emulation of the swing equation characteristic of the SG, providing damping and inertia for stability [4]. VSGs may possess low-frequency oscillations, sub-synchronous resonance, and synchronous resonance due to interactions with elements in the electrical grid [6]. Unlike SGs in power systems, inverters possess fast actuation while lacking sufficient inertia making the interactions between controllers and line dynamics more profound which may lead to instabilities [7]. While inertia can be emulated in the VSG, it is desirable in small signal stability but aggravates transient synchronisation stability. On the other hand, damping is pivotal in low inertia, inverter-dominated grids, enhancing both small signal and large signal stability [9].

To achieve spectra of digital control applications in VSGs, virtual impedance (VI) has been implemented in various ways, and at different locations in the VSC control structure [10]. For example, VI applied in series

<sup>1</sup> Department of Electrical Power Engineering, Faculty of Engineering, Egypt-Japan University of Science and Technology, New Borg El-Arab City, Alexandria 21934, Egypt

<sup>2</sup> Department of Electrical Engineering, Faculty of Engineering, Aswan University, Aswan 81542, Egypt

<sup>3</sup> Department of Electrical Engineering, Faculty of Engineering, Mansoura University, El-Mansoura 35516, Egypt

<sup>4</sup> Department of Electrical Engineering, Faculty of Information Science and Electrical Engineering, Kyushu University, Fukuoka 819-0395, Japan

<sup>5</sup> Department of Electrical Power and Machines Engineering, Faculty of Engineering, Tanta University, Tanta 31511, Egypt  
emmanuel.ebinyu@ejust.edu.eg, omar.abdelrahim@ejust.edu.eg, sobhy.abdelkader@ejust.edu.eg,  
shoyama@ees.kyushu-u.ac.jp, diaa.mansour@ejust.edu.eg

with the outer impedance of the LC filter achieves power-sharing enhancement, and improvement of the  $X/R$  ratio of the grid impedance to achieve decoupled control of the active and reactive power in droop control [11]. Virtual impedance current limitation has been designed for overcurrent protection of the power electronics in converters [13]. Whereas virtual resistance (VR) can be applied in LC resonance suppression and harmonic mitigation in VSCs [15], this article focuses on its use in system damping to suppress synchronous frequency resonance (SFR) present in the fundamental power signals of VSGs in low  $R/X$  systems. SFR threatens the stability of VSGs when high amplitude oscillations appear near the synchronous frequency and should therefore be eliminated [16]. By increasing system damping through increasing the resistive part of the impedance, SFR can be suppressed, with VR preferred to grid resistance for power efficiency purposes [18]. VI has also been used to suppress power oscillations in multi-VSG grids, being applied adaptively to eliminate the frequency differences which cause oscillation in microgrids [19].

The application of VR to enhance transient synchronisation stability has taken on many approaches in literature. Transient VR is used to suppress resonance oscillations [20], with a high pass filter used to avoid coupling in the steady state caused by increased resistive impedance, especially in stiff grids. VR has also been applied to suppress oscillations that appear in GFMs postfault, with a fixed VR scheme proposed in [21] and an adaptive scheme as proposed in [22]. However, the application of VR in VSGs has a negative effect on large disturbance stability, narrowing the possible overshoot angle range of the power angle. A power reference reduction method based on the voltage drop magnitude was subsequently proposed to eradicate this anomaly in [23]. It remains desirable in VSGs to improve transient stability, especially in inverter-dominated grids, and many approaches have been explored to address this issue. In [24], the positive feedback modes of the power angle control which represent instability are adaptively switched to the negative modes to keep the VSG operational even beyond the critical clearing time of the VSG under fault. Ref. [25] proposed an angle estimation method to adaptively control the transient stability of a GFM based on the virtual orthogonal power. A transient damping method, dependent on the frequency difference between the grid and the VSG is proposed in [26] and is designed to harmonise inertia response and synchronisation stability in the presence of high inertia. In [27], a design-oriented study of second-order GFMs such as the VSG reveals that the damping factor plays a key role in transient stability in comparison to the inertia term. The reactive power loop

can also be used to enhance the transient stability, with methods proposed in [28]. In [30], the VSG structure is modified to include a PI controller and virtual power feedback in the active power loop to enhance the operation of VR in the transient stability of the VSG. However, there is no analytical explanation for the case of the virtual power feedback, apart from graphical analysis using attraction regions.

In this article, the virtual power concept is adopted to track the power reference during transients, showing a better performance than active power tracking, producing better transient synchronization stability performance of the VSG. The VSG incorporates the VR in the steady state to suppress synchronous oscillations through the improvement of the damping of the line dynamics, retaining its conventional structure in the steady state, while transforming to apply virtual power in the active power loop to improve the transient angle stability and thereby improving the transient stability of the system. The analytical equivalent damping of the proposed method is derived, being a function of the VR, the inverter voltage and the grid voltage for practical application.

The emphasis in this article is on the transient angle stability of the VSG, which differs from transient voltage stability [31], in the transient synchronisation stability, based on the use of VR damping. The concept of virtual point of common coupling (PCC) is adopted to show the effect of the conventional use of VR on transient stability, and virtual power feedback is implemented under fault conditions. This is shown to have equivalence to VR damping which enhances transient stability.

Other sections in this article are organized as follows: Section 2 stipulates the application of VR in VSG to suppress resonance oscillations in the small signal stability. In Section 3, the power transfer characteristics of the VSG with VR are derived, using the concept of virtual PCC. The proposed method is presented in Section 4 with subsequent analysis to show its efficacy. The concluding Section 5 includes the simulation set-up and results in MATLAB/Simulink showing improved transient synchronization stability of the proposed method compared to conventional VSG.

## 2 Application of virtual resistance in VSG

Figure 1 shows the layout of the VSG GFM inverter, modelled in the synchronous rotating frame ( $dq$ ) to necessitate controller design. VR is included as  $R_v$  in the power loop.

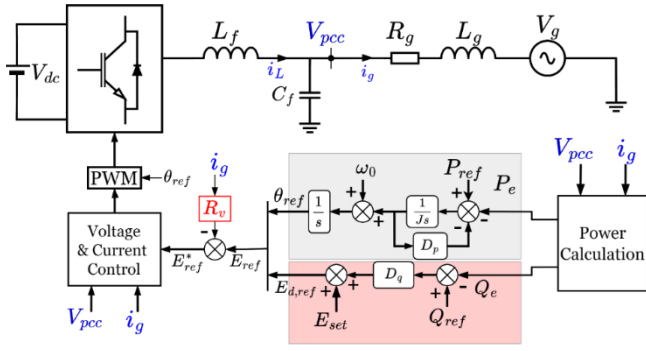


**Fig. 1.** Schematic layout of Virtual Synchronous Generator

## 2.1 VSG description

The structure contains the outer power loops consisting of the active power loop (APL) and reactive power loops (RPL), inner voltage and current controller whose bandwidth is designed higher than the outer loops to ensure their transparency when modelling grid interactions with the VSG outer loop. The connected grid is modelled by a voltage source with a constant voltage  $V_g \angle \theta_g$  and a series impedance containing line resistance  $R_g$  and inductance  $L_g$ .

The VSC is modelled with a constant DC bus when considering the interaction on the grid-facing side, given energy storage and intermittent renewables supplying the DC bus can be controlled to supply steady DC power [32]-[35], which is approximated as constant. An LC filter is added to the VSC at the PCC to interface with the grid.

The PCC voltage  $V_{pcc}$  is assumed to track the reference voltage,  $E_{ref}^*$  with the outer loop bandwidth much smaller compared to that of the inner controllers, making their effect negligible.  $V_{pcc} = V_{pcc} \angle \theta_{pcc}$  is the voltage vector at the PCC while  $V_g = V_g \angle \theta_g$  is the grid voltage vector. The phase difference between these two vectors is  $\delta = \theta_{pcc} - \theta_g$  with the grid voltage vector taken as the reference aligned with the  $d$ -axis of the rotating frame of the converter.  $\theta_g = \omega_g t$ , where  $\omega_g$  is the nominal grid frequency.

The APL is derived from the swing equation and adjusts the angular frequency based on real power feedback using the relationship

$$\omega = \omega_0 + \frac{1}{Js + D_p} \cdot (P_{ref} - P_e) \quad (1)$$

where  $\omega_0$  is the set frequency equal to the grid frequency  $\omega_g$ ,  $J$  is the virtual inertia term,  $D_p$  is the damping term, which is the reciprocal of the droop value,  $P_{ref}$  is the reference power,  $P_e$  is the real output power at the PCC.

The RPL follows a droop relationship between the PCC voltage and the reactive power, with the reactive power feedback implemented for reactive power sharing [36]. This is given by

$$E_{d,ref} = E_{set} + D_q(Q_{ref} - Q_e) \quad (2)$$

where  $E_{set}$  is the set value of the grid voltage,  $D_q$  is the droop coefficient,  $Q_{ref}$  is the reference reactive power, and  $Q_e$  is the reactive power at the PCC.

$P_e$  and  $Q_e$  are obtained by feeding the instantaneous power  $\tilde{p}$  and  $\tilde{q}$ , given by (3) through low pass filters with the cutoff frequency  $\omega_c$  to remove high-frequency components in the power signals. The delivered signals into the control loops are therefore fundamental components.

$$\tilde{p} = V_d^{pcc} i_{gd} + V_q^{pcc} i_{gq} \quad (3a)$$

$$\tilde{q} = V_d^{pcc} i_{gq} - V_q^{pcc} i_{gd} \quad (3b)$$

$$P_e = \frac{\omega_c}{s + \omega_c} \tilde{p}, \quad Q_e = \frac{\omega_c}{s + \omega_c} \tilde{q} \quad (4)$$

VR is implemented as a voltage drop on the reference voltage according to (5) and (6), to effectively be in series with the grid impedance  $R_g + j\omega_g L_g$  by using the grid current,  $i_g = [i_{g,d} \ i_{g,q}]^T$  as the feedback signal [10][30].

$$E_{d,ref}^* = E_{d,ref} - i_{g,d} R_v \quad (5)$$

$$E_{q,ref}^* = 0 - i_{g,q} R_v \quad (6)$$

Due to this implementation, the application of VR is limited to the bandwidth of the voltage controller, given that it alters the reference input value for the voltage controller of the PCC voltage. VR may be applied at different points in the VSC according to the purpose of design [10], however, in the case of grid interactions, VR is implemented in series with grid impedance.

## 2.2 Virtual resistance in small signal stability

Dynamic modelling is preferred to static modelling in the small signal analysis of VSGs to incorporate the effect of the fast actuation of power electronics [37]. In the case when the power system is dominated by mechanical rotary machine dynamics which are slow in comparison to the line dynamics, then phasor modelling is sufficient. The dynamics at the PCC for the circuit in Fig. 1 are given by

$$V_{PCC,dq} - V_{g,dq} = L_g \frac{di_{g,dq}}{dt} + R_g i_{g,dq} + j\omega L_g \cdot i_{g,dq} \quad (7)$$

where  $V_{PCC} = [V_d \ V_q]^T$ ,  $V_{g,dq} = [V_g \ 0]^T$ ,  $i_g = [i_{g,d} \ i_{g,q}]^T$ .

Then, the complex power,  $S$  at the PCC follows (8) according to the instantaneous power theory.

$$S = 1.5 \cdot V_{PCC,dq} \cdot i_{g,dq}^* = P_e + jQ_e \quad (8)$$

where  $i_{g,dq}^*$  is the conjugate of the grid current  $i_{g,dq}$ .

By taking the Laplace transform of (7) and applying linearisation about an operational point denoted by subscript "0", the small signal model of the output power  $P_e$  and  $Q_e$  can be expressed by a state matrix relating  $\Delta P_e, \Delta Q_e$  to  $\Delta \delta, \Delta E$ . The transfer functions are derived and expressed in the matrix system by

$$\begin{bmatrix} \Delta P \\ \Delta Q \end{bmatrix} = \begin{bmatrix} H_{P\delta} & H_{PV} \\ H_{Q\delta} & H_{QV} \end{bmatrix} \begin{bmatrix} \Delta \delta \\ \Delta E \end{bmatrix} \quad (9)$$

where the transfer functions  $H_{P\delta}, H_{PV}, H_{Q\delta}, H_{QV}$  are given as

$$H_{P\delta} = \frac{\Delta P}{\Delta \delta} = \frac{V_{PCC} V_g X_g \cos \delta_0 + (sL_g + R)V_{PCC} V_g \sin \delta_0}{(sL_g + R_g)^2 + X_g^2} \quad (10)$$

$$H_{PV} = \frac{\Delta P}{\Delta V} = \frac{(sL_g + R_g)(2V_{PCC} - V_g \cos \delta_0) + V_{PCC} X_g \sin \delta_0}{(sL_g + R_g)^2 + X_g^2} \quad (11)$$

$$H_{Q\delta} = \frac{\Delta Q}{\Delta \delta} = \frac{-(sL_g + R_g)V_{PCC} V_g \cos \delta_0 + V_{PCC} V_g X_g \sin \delta_0}{(sL_g + R_g)^2 + X_g^2} \quad (12)$$

$$H_{QV} = \frac{\Delta Q}{\Delta V} = \frac{-(sL_g + R_g)V_{PCC} \sin \delta_0 + X_g(2V_{PCC} - V_g \cos \delta_0)}{(sL_g + R_g)^2 + X_g^2} \quad (13)$$

It is deduced from the transfer functions of the Jacobian matrix in (9) that a pair of conjugate poles exists in the system given by

$$s_{1-2} = -\frac{R_g}{L_g} \pm j\omega_0 \quad (14)$$

where  $\omega_0$  represents the synchronous frequency equal to the grid frequency. The location of the poles  $s_{1-2}$  in the complex cartesian plane determines the stability of the system according to eigenvalue analysis [38]. The poles, being complex conjugate, represent the existence of oscillatory modes whose characteristic depends on the real and imaginary parts. When the ratio  $R_g/L_g$  is small, translating in a small damping ratio, the system drifts into potential instability characterised by amplitude excursions with oscillations at the synchronous frequency  $\omega_0$  owing to the shifting of the poles towards the imaginary axis. Therefore, SFR in small signal stability of GFMs manifests as oscillations around the grid frequency with  $-180^\circ$  phase jumps which cause system instability. The system damping ratio with eigenvalues given in (14) determines the rate of decay of oscillation amplitude and is given by

$$\zeta_{s_{1-2}} = \frac{R_g}{\sqrt{R_g^2 + (L_g \omega_0)^2}} \quad (15)$$

By increasing the magnitude of the real part of  $s_{1-2}$ , the damping of the system can be increased, thereby

suppressing oscillations. For this purpose, VR is used in preference to real resistance due to power efficiency purposes according to (16).

$$\zeta_{s_{1-2}}^* = \frac{R_g + R_v}{\sqrt{(R_g + R_v)^2 + (L_g \omega_0)^2}} \quad (16)$$

The synchronous resonance phenomenon is demonstrated in Fig. 2(a) where VR is reduced from 0.05 p.u. to 0.001 p.u. in a VSG connected to the grid at  $t = 2$  seconds. From the waveforms, instability is observed in the P and Q waveforms owing to instability due to insufficient damping in the system. The suppression of resonant peaks of the system by the adoption of VR is shown by bode plots in Fig. 2(b).

### 2.3 Designing VR for VSG damping application

The design of VR falls under VI design which considers the power transfer capacity of the generator, the P-Q decoupling coefficient to maintain droop operation of the APL and RPL, and the desired damping of the system to ensure stability [11]. In this article, given the small  $R/X$  value of the grid ( $\frac{R_g}{\omega_0 L_g} = 0.04$ ), the value of  $R_v$  chosen must keep this ratio within a desirable range to ensure decoupled APL and RPL. The system damping is also given consideration, being deduced from (17) based on eigenvalue analysis of the power transfer characteristics [11].

$$R_v = \frac{\zeta_{s_{1-2}}^* (\omega_0 L_g)}{\sqrt{1 - \zeta_{s_{1-2}}^*{}^2}} - R_g \quad (17)$$

Considering the system parameters used in this article, Table 1 shows the system damping and  $R/X$  ratio for the values of  $R_v$  used. Damping is required between  $0.1 < \zeta_{s_{1-2}} < 0.7$  for an underdamped system with appropriate rise time and asymptotic stability while the  $R/X$  ratio is desired to remain as low as possible.

**Table 1.** VR values and related damping and  $R/X$  ratio

$R_v$ (p.u.)	$\zeta_{s_{1-2}}^*$	$(R_g + R_v)/X$
0.01	0.06	0.06
0.02	0.08	0.08
0.05	0.14	0.14
0.1	0.23	0.24
0.2	0.40	0.44

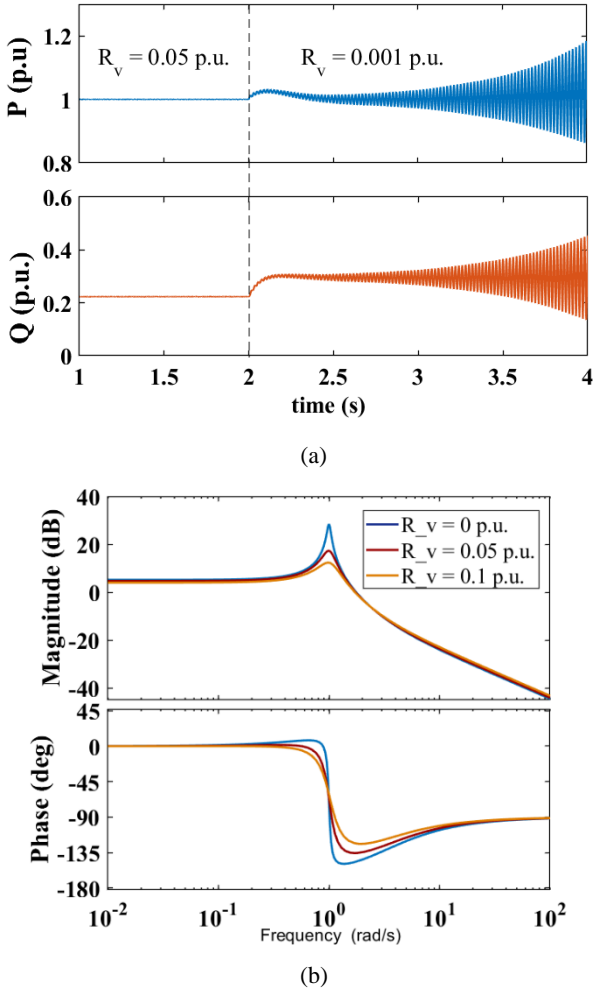


**Fig. 2.** (a) Synchronous resonance when VR changes from 0.05 p.u. to 0.001 p.u. (b) Bode plot of  $H_{P\delta}$  to demonstrate the suppression effect of VR in the steady state.

### 3 Effects of VR on the power transfer characteristics of VSG

The insertion of VR in the control structure in Fig. 1 affects the voltage at the PCC,  $V_{pcc}$ . Without VR,  $V_{pcc}$  easily directly follows its reference  $E_{ref}$  assuming the transparency of the inner control loops. With VR, the voltage drop implemented to model the effect of resistance changes the relationship between the reference voltage,  $E_{ref}$ , and  $V_{pcc}$ , so that  $V_{pcc}$  now tracks  $E_{ref}^*$ . Accordingly, it becomes difficult to model power relationships between  $P_e$  and  $\delta$  using the VSC parameters to sufficiently study the  $P_e - \delta$  characteristics [23]. For this purpose, the internal VSG is adopted for analysis which gives rise to the concept of virtual PCC. This is illustrated in Fig. 3.

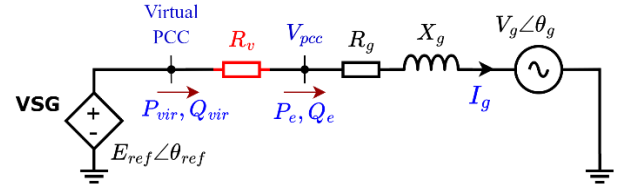


**Fig. 3.** Equivalent circuit layout of the VSG considering the virtual PCC

#### 3.1 Modelling $P_e$ and $Q_e$ using the virtual PCC

Consider the equivalent circuit diagram in Fig. 3 of the VSG with  $R_v$  connected to the grid. The use of virtual PCC considers the inner VSG denoted by the vector  $E_{ref} \angle \theta_{ref}$ . The virtual PCC with respect to the grid has an angle  $\delta_{vir} = \theta_{ref} - \theta_g$ . In the presence of VR,

$$V_{pcc} e^{j\delta} = E_{ref} e^{j\delta_{vir}} - R_v \cdot \frac{E_{ref} e^{j\delta_{vir}} - V_g}{R_v + R_g + j\omega X_g} \quad (18)$$

Therefore, the expressions for the power at the virtual PCC and that injected into the grid are given by the (19) to (21) at the bottom of the next page. From the expressions, it is observed that the introduction of  $R_v$  alters the power transfer equations at the PCC ideally, which has consequences on the characteristics of power at the PCC, as shown in the next section.

#### 3.2 Effects of $R_v$ on the transient stability of VSG

Primarily in power systems, transient angle stability is related to the dynamics of the power angle  $\delta$  upon a large disturbance [27]. Given that overcurrent saturation techniques are used in GFM during faults, transient stability is considered for instances where the current saturation is not triggered, as this would result in a different analysis [26]. A voltage sag is the type of disturbance considered therefore, given it is commonplace in weak grids [23]. It is necessary to sustain synchronization of GFMs for fault-ride through or extend the critical clearing time so that the protection systems of the grid can clear the fault within the acceptable time. Using the traditional  $P - \delta$  relationship, the transient stability is analysed using the equal area criterion and is intuitively analysed using the critical clearing angle and the critical clearing time [38]. Then, transient stability is categorized based on the existence of equilibrium points on the  $P - \delta$  curve during and after the fault. When a fault causes a change in the power transfer of the VSG, the  $P - \delta$  curves in Fig. 4 show the possible outcomes. The occurrence of a fault will alter the positions of equilibrium points, categorised as stable equilibrium point (SEP) or unstable equilibrium point (UEP), either causing their existence as shown in Fig. 4(a) or their non-existence as shown in Fig. 4(b).

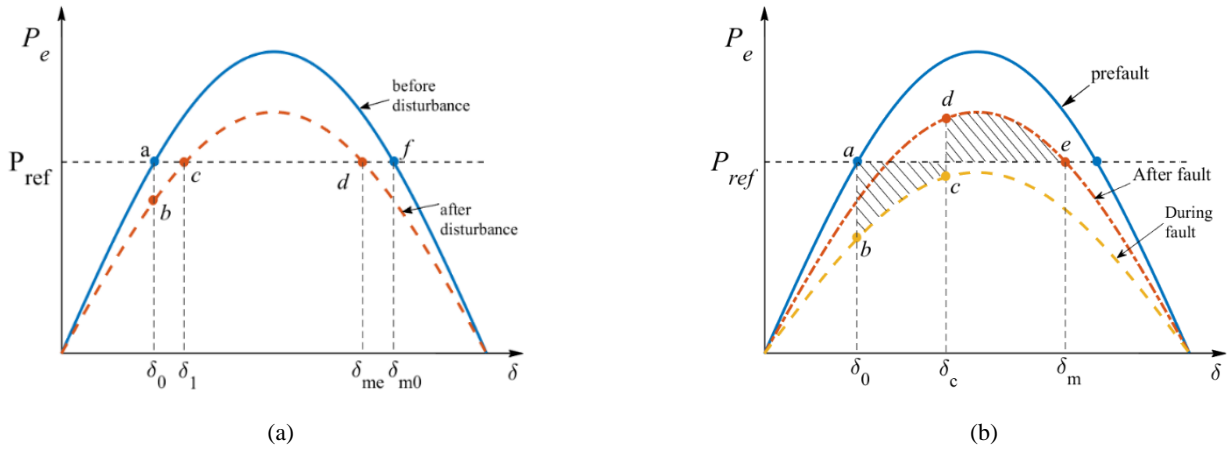


**Fig. 4.** Types of transient synchronisation stability scenarios: (a) Type 1 in which there is the existence of equilibrium points after the disturbance (b) Type 2, in which the fault causes the non-existence of equilibrium points and subsequently the need for equal area analysis.

Figure 4(a) shows the behaviour of the system when a disturbance causes a reduction in power transmitted, but the system remains stable because of the transition from point ‘a’ to ‘b’ to ‘c’, where ‘a’ is the SEP before disturbance, and ‘c’ is the SEP after the disturbance. This therefore represents systems that remain stable even when a disturbance is present. Fig. 4(b) shows the instance when the fault causes the transmitted power to fall below the reference power, and thus the non-existence of equilibrium points. When the system dynamics follow the path ‘a’ to ‘b’, the system starts to accelerate towards the point ‘c’. When this happens, it is critical to clear the fault before point ‘c’ which represents the critical clearing point beyond which the angle dynamics accelerate out of control, and instability ensues.

The  $P_e - \delta_{vir}$  relationship can be derived comprehensively by replacing  $E_{ref}$  in (21).  $E_{ref}$  is a function of the power angle  $\delta_{vir}$  as shown in (22), with the expression derived by replacing  $Q$  in (2) with the expression in (20). Therefore, the  $P_e - \delta_{vir}$  curves for the VSG, using the expression of  $P_e$  derived by replacing

$E_{ref}$  in (21) by (22) are plotted in Fig. 5 with different values of  $R_v$  to illustrate the effect of VR on the angle overshoot range, which represents the range of excursions of the angle  $\delta_{vir}$  without the loss of synchronism.

The  $P_e - \delta_{vir}$  characteristics for different combinations of grid resistance  $R_g$  and virtual resistance  $R_v$  are plotted to establish the effect of each parameter on the maximum transferable power, represented by the peak of the curve, and the angle difference between the SEP and UEP which represents the overshoot angle range. From Fig. 5, it is observed that  $R_g$  increases the maximum transferable power and enlarges the angle range displayed by Case 2 and Case 3. On the other hand,  $R_v$  reduces the maximum power and narrows the available angle range for overshoot which is the case for Case 4 and Case 5. With a decreasing overshoot angle range, the tendency to loss of synchronism increases, showing that  $R_v$  negatively affects the power angle dynamics when the active power at the PCC  $P_e$  is designed to track its reference  $P_{ref}$  with VR installed.

$$P_{vir} = 1.5 \cdot \frac{X_g E_{ref} V_g \sin \delta_{vir} + (R_g + R_v)(E_{ref}^2 - E_{ref} V_g \cos \delta_{vir})}{(R_g + R_v)^2 + X_g^2} \quad (19)$$

$$Q_{vir} = Q_e = 1.5 \cdot \frac{X_g (E_{ref}^2 - E_{ref} V_g \cos \delta_{vir}) - (R_g + R_v) E_{ref} V_g \sin \delta_{vir}}{(R_g + R_v)^2 + X_g^2} \quad (20)$$

$$P_e = P_{vir} - \frac{2}{3} \cdot \left( \frac{P_{vir}^2 + Q_{vir}^2}{E_{ref}^2} \right) \cdot R_v = \frac{3 R_v (E_{ref} V_g \cos \delta_{vir} - V_g^2) + X_g E_{ref} V_g \sin \delta_{vir} + R_g (E_{ref}^2 - E_{ref} V_g \cos \delta_{vir})}{(R_g + R_v)^2 + X_g^2} \quad (21)$$

$$E_{ref} = \frac{1.5 V_g D_q \alpha \cos \delta_{vir} + 1.5 D_q \beta V_g \sin \delta_{vir} - 1 + \sqrt{(1.5 V_g D_q \alpha \cos \delta_{vir} + 1.5 D_q \beta V_g \sin \delta_{vir} - 1)^2 + 6 D_q \alpha (E_{set} + D_q Q_{ref})}}{3 \alpha D_q} \quad (22)$$

$$\text{where } \alpha = \frac{X_g}{(R_g + R_v)^2 + X_g^2}, \beta = \frac{R_g + R_v}{(R_g + R_v)^2 + X_g^2}$$

The dynamic response of the power angle can be more qualitatively studied using the phase portrait [27] which quantifies the behaviour of  $\dot{\delta}_{vir} - \delta_{vir}$  and further entrenches the findings in the  $P_e - \delta_{vir}$  curves. In the Fig. 6, two cases are narrowed out: Case 4 with  $R_v = 0.02$  p.u. and  $R_g = 0$  p.u. and Case 1 with  $R_g = 0.1$  p.u. and  $R_v = 0$  p.u. It is observed that the application of VR narrows the range of the angle overshoot, which is the difference between the SEP denoted by subscript ‘e’ and the UEP denoted by ‘m’. From Fig. 6,  $\delta_{em1}$  for Case 1 without VR is a greater overshoot range and represents better dynamic performance than  $\delta_{em4}$  for Case 4. It is also observed on the  $\delta_{vir} -$  axis of Fig. 6 that there is a decreasing angle overshoot with an increased magnitude of  $R_v$ , which points to the increased transient instability with VR magnitude increase. Also, on the  $\Delta\omega -$  axis, trajectories of the phase portrait show that increased  $R_v$  leads to greater differentials which is an indication that the application of VR in the conventional way jeopardizes the frequency stability of the VSG. Cases 5 and 6 are also considered where the application of  $R_v = 0.05$  p.u. and  $R_v = 0.1$  p.u. cause instability in the dynamics of the VSG upon a voltage sag from 1 to 0.65 p.u. of the grid voltage. These cases show that the application of  $R_v$  can cause instability, even when designed to damp oscillations within the critical damping range in the steady state.

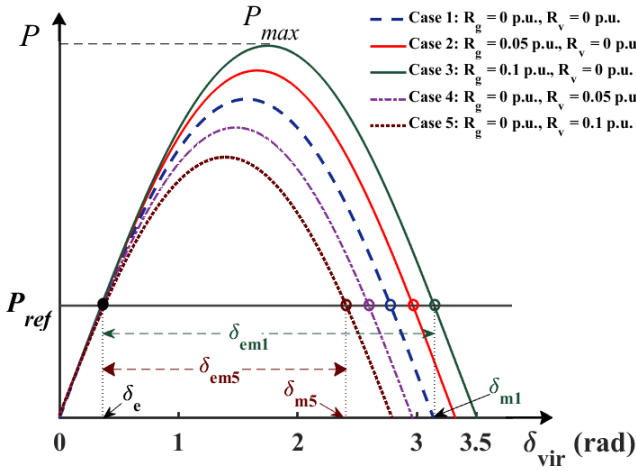


**Fig. 5.** Effect of  $R_g$  and  $R_v$  on the  $P - \delta_{vir}$  curve

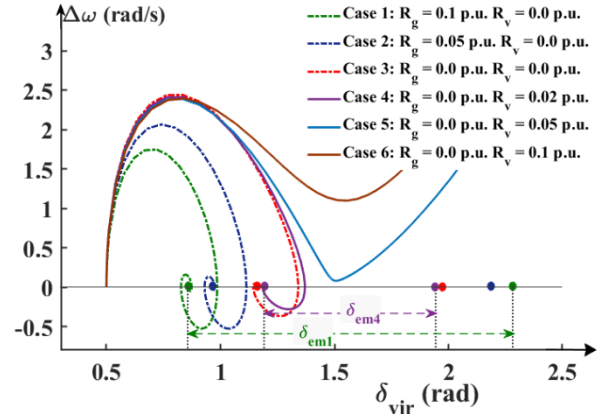


**Fig. 6.** Phase portrait showing the  $\dot{\delta}_{vir} - \delta_{vir}$  behaviour when the  $V_g$  drops from 1 p.u. to 0.65 p.u. with  $J = 5$  p.u. and  $D_p = 25$  p.u.

#### 4 Proposed improvement in VSG during voltage sag

Based on the observed effects of VR such as reduction in angle overshoot, and the increased maximum frequency deviations, it is expedient to design the VSG to retain VR in the steady state, while averting its detrimental impact on the transient stability.

##### 4.1 Modification in VSG

By introducing the virtual power given by (23) in the active power loop during fault conditions (transient periods), the VSG is modified as shown in Fig. 7.

$$P_{vir} = 1.5 (E_{refd} \cdot i_{gd} + E_{refq} \cdot i_{gq}) \quad (23)$$

where  $E_{refd}$ ,  $E_{refq}$  are the  $dq$  components of the voltage at the virtual PCC in Fig. 3. Equation (23) is the controller implementation of (19).

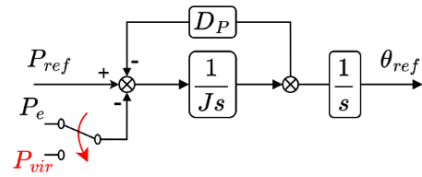


**Fig. 7.** The modification in VSG with  $P_{vir}$  applied as the power tracking variable instead of  $P_e$  upon a fault to provide damping for transient synchronisation stability

The switchover from  $P_e$  to  $P_{vir}$  is activated upon fault detection, using methods that are beyond the scope of this article but are widely covered elsewhere [22][39].

Compared with the modified VSG introduced in [30] which incorporates a PI controller and virtual power  $P_{vir}$  negative feedback in the power loop and designed to track the power reference in the steady state, the proposed method eliminates the PI controller which takes away the need for tuning, and the pole introduced by the PI which can cause instability in the closed loop. The proposed method retains the conventional VSG in the steady state, with the active power loop control law given by (1). In the transient state, when the fault has been detected, the  $P_{vir}$  is activated into the VSG changing the APL control law to

$$\omega = \omega_0 + \frac{1}{Js+D_p} \cdot (P_{ref} - P_{vir}) \quad (24)$$

When the grid voltage falls below 0.95 p.u. to imply a voltage sag [23], with the acceptable range of voltage stability, the controller is set to implement virtual power to replace the real power in the VSG in tracking the power reference, to change the power angle dynamics of the VSG.

As shall be elaborated in the next section (Section 4.2), it is shown that the proposed method is equivalent to a VR damping method for transient stability.

The use of  $P_{vir}$  in the transient period and not during normal operation is based on the need for real power  $P_e$  to track its reference  $P_{ref}$  in the steady state which is a requirement for GFM DERs in order to supply the necessary power according to demand up-to the rated capacity. In the transient period, synchronisation stability is given priority to keep the generator online. The IEEE Standards 1547-2018 [40] necessitate that distributed energy generators (DERs) keep the supply of power for a while, but they do not explicitly ascribe that normal power rating should be maintained. This interpretation has led to the use of power reference reduction methods to enhance synchronisation stability in [23].

Therefore, the use of  $P_{vir}$  in the VSG for transient synchronisation stability will reduce the transferred power  $P_e$  according to Fig. 8. This is evident in the expressions of  $P_e$  and  $P_{vir}$ . While using  $P_{vir}$  in the APL, the power transferred ( $P_e$ ) is sufficient in this transient phase which only usually lasts for a few cycles while priority is placed on synchronisation stability.

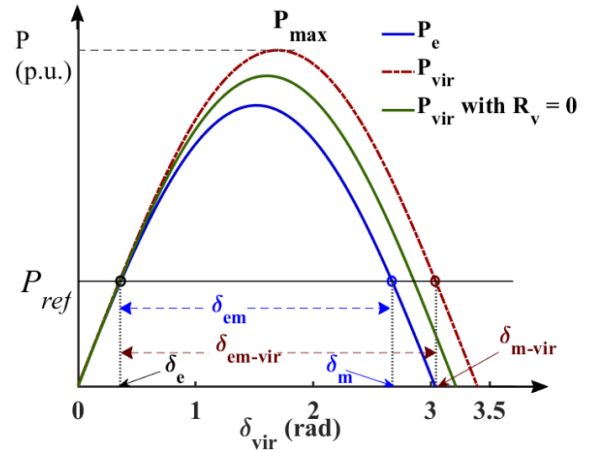


**Fig. 8.** Comparison between  $P_e$  and  $P_{vir}$  to show the difference in the overshoot range for each power tracking parameter.

In Fig. 8, the curves of  $P_e$ ,  $P_{vir}$ , and  $P_{vir}(R_v = 0)$  terminate at different points on the  $\delta_{vir}$  - axis due to the power dissipation and the power angle due to the real part of the impedance,  $Z = (R_g + R_v) + jX_g$ , for the different power configurations effected between the virtual PCC and the grid.

#### 4.2 The damping effect of using $P_{vir}$ in the VSG during transient synchronisation

Consider the VSG control law in (1) rewritten for emphasis below.

$$J\dot{\omega} = P_{ref} - P_e(\delta_{vir}) - D_p(\omega - \omega_0) \quad (25)$$

$$\dot{\delta}_{vir} = \omega \quad (26)$$

Rewriting to express (25) and (26) into a second-order equation,

$$\ddot{\delta}_{vir} = \frac{P_{ref}}{J} - \frac{P_e(\delta_{vir})}{J} - \frac{D_p(\dot{\delta}_{vir} - \omega_0)}{J} \quad (27)$$

where  $P_e(\delta_{vir})$  is given by (21).

For simplification of the analysis, let the assumption  $X_g \gg (R_v + R_g)$  hold for the grid impedance, so that  $\delta_{vir} \approx 0$ ,  $\cos \delta_{vir} \approx 1$  and  $\sin \delta_{vir} \approx \delta_{vir}$ . Equation (27) can therefore be summarised as

$$J\ddot{\delta}_{vir} = P_{ref} - \frac{E_{ref}V_g}{X_g}\delta_{vir} - D_p(\dot{\delta}_{vir} - \omega_0) \quad (28)$$

Simplifying (28) by taking the Laplace transform, it is expressed to emphasize the second-order characteristic behaviour as

$$\delta_{vir} = \frac{P_{ref} + D_p\omega_0}{Js^2 + D_p s + \frac{E_{ref}V_g}{X_g}} \quad (29)$$

Therefore, the damping ratio of the angle characteristics,  $\zeta$ , of the VSG system, can be approximated as

$$\zeta = \frac{D_p}{2} \sqrt{\frac{X_g}{J E_{ref} V_g}} \quad (30)$$

The damping term  $D_p$  is an avenue to improve the transient stability of the VSG as shown in (29), where it is directly proportional to the damping ratio of the second order system and its increase has the effect of reducing the overshoot of the angle characteristics, subsequently increasing the range of the acceptable angle overshoot. This is not the case with virtual inertia,  $J$ . From (30), increase in  $J$  decreases the damping ratio of the second order system which is detrimental to transient stability. Therefore, it is more attractive to increase the effective damping term as compared to the virtual inertia term to improve transient stability.

Consequently, an additional damping term resulting from the proposed method should be responsible for the transient stability improvement. This is derived below.

By adopting  $P_{vir}$  instead of  $P_e$ , the control law of the VSG can be expressed as

$$J\omega = P_{ref} - (P_e(\delta_{vir}) + D_{P,R_v}) - D_p(\omega - \omega_0) \quad (31)$$

where

$$P_{vir} = P_e(\delta_{vir}) + D_{P,R_v} \quad (32)$$

$$D_{P,R_v} = 1.5 \cdot \frac{R_v (E_{ref}^2 + V_g^2 - 2E_{ref}V_g \cos \delta_{vir})}{(R_v + R_g)^2 + X_g^2} \quad (33)$$

The use of  $P_{vir}$  introduces a damping term,  $D_{P,R_v}$  as shown in (31) which is proportional to the VR as indicated in (32) and (33). The proposed method can thus improve the transient stability of the VSG due to the damping term,  $D_{P,R_v}$  being effectively introduced. Therefore, VR can be used to offer damping both in the steady state and during transients with the proposed method, harnessing the advantages presented by VR for oscillation damping. In non-ideal situations where the virtual PCC is inaccessible and therefore  $E_{ref}$  non-measurable, the damping term  $D_{P,R_v}$  can be derived using the PCC voltage,  $V_{pcc} \angle \delta$ , assuming  $V_{pcc} \approx E_{ref}$  and  $\delta \approx \delta_{vir}$  giving,

$$D_{P,R_v} = 1.5 \cdot \frac{R_v (V_{pcc}^2 + V_g^2 - 2V_{pcc}V_g \cos \delta)}{(R_v + R_g)^2 + X_g^2} \quad (34)$$

The  $\dot{\delta}_{vir} - \delta_{vir}$  characteristics of (25) and (26) can be studied using the phase portrait to further study the dynamic behaviour of the system.

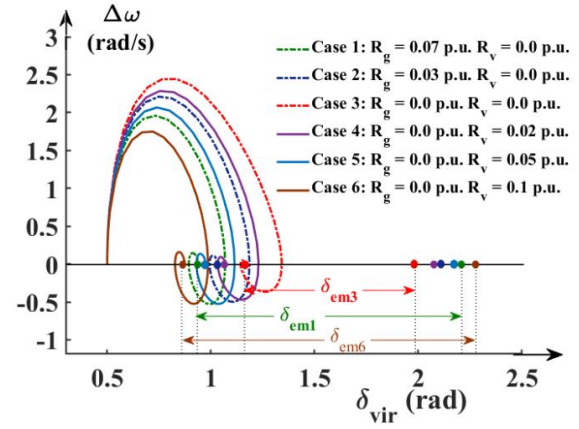


**Fig. 9.** Phase portrait showing the performance of the proposed implementation when the grid voltage falls to 0.65 p.u.

Figure 9 reveals the existence of equilibrium points in the phase portrait with increasing VR for the virtual power proposed method, revealing the damping effect of the method as demonstrated in (31). For comparison, consider the Case 1 ( $R_g = 0.07$  p.u.,  $R_v = 0.0$  p.u.), Case 3 ( $R_g = 0.0$  p.u.,  $R_v = 0.0$  p.u.) and Case 6 ( $R_g = 0.0$  p.u.,  $R_v = 0.1$  p.u.).

Case 1 reveals the effect of  $R_g$  on the angle overshoot range, as compared to Case 3 where  $R_g = 0.0$  p.u. and  $R_v = 0.0$  p.u., with the overshoot range increasing with  $R_g$  which is an indication of improved transient performance. This case is the conventional standpoint where the grid resistance increases the maximum power transferred during a fault as well as introduces damping. Comparing Case 6 and Case 3, it is observed that with an increase in  $R_v$ , there is the same effect as  $R_g$ , with the angle overshoot range increasing with increasing  $R_v$ . Therefore, with the proposed method of improving the transient stability using the VR, it is observed that the VR has the same effect as the grid resistance. With increase in  $R_v$  is monitored a subsequent increase in angle overshoot range and a reduction of the frequency deviation. The effect of this results in better transient stability and frequency stability of the VSG. This differs from the analysis provided in Section 3.2 where VR exacerbates transient stability and frequency stability when used in the convention way. The phase portrait therefore reveals that the proposed modification improves the transient response of the VSG when subjected to a voltage sag.

## 5 Simulation and results

The model in Fig. 1 is built in MATLAB/Simulink using the parameters shown in Table 2. A 10 kVA system is modelled, connecting to a power grid with a short circuit ratio (SCR) of 2, which represents a weak grid, representative of an inverter-dominated power grid.

The grid disturbance applied to the system is a voltage sag symmetrical to all the phases of the grid line voltage, being the most severe fault categorised by phase jumps and voltage magnitude reduction. The voltage sag is a suitable transient event that permits continued supply of power as required by the IEEE Standard 1547-2018 [40] for DERs. Faults of 0.6 p.u. and 0.5 p.u. are considered to provide the different scenarios of transient stability with the value of  $R_v$  varied from 0.01 p.u. to 0.1 p.u. to show how the value of VR affects the conventional VSG and the proposed modified VSG performances.

The control system is set to trigger, switching to the proposed modification in the VSG algorithm when the voltage threshold of 0.95 p.u., being the lower allowable limit of the generator voltage and signifying a voltage sag, has been crossed through the measurement of the grid voltage drop.

Parameters  $D_p$  and  $D_q$  are chosen considering the required grid codes, for stipulated droop functionalities of the APL and the RPL. The virtual inertia parameter  $J$  is also chosen to establish the required rate of change of frequency limits. Upon the occurrence of the voltage sag, the active power ( $P$ ), PCC voltage angle ( $\delta$ ), grid current for phase 'a' ( $i_{ga}$ ), frequency ( $f$ ), and the PCC voltage ( $V_{pcc}$ ) are monitored. It is assumed that the operation of current saturation is not triggered in the transient phase of the operation to fully comprehend the significance of the proposed method over the conventional VSG.

**Table 2.** VSG system parameters used in Simulation

Parameters	Description	Value	p.u.
$S_{ref}$	Base Power	10 kVA	1
$P_{ref}$	Active Power ref.	10 kW	1
$Q_{ref}$	Reactive Power ref.	0	0
$f_c$	Filter cutoff freq.	2 Hz	0.04
$V_g/V_{base}$	Grid voltage	311 V	1
$\omega_0$	Frequency	$100\pi$ rad/s	1
$L_g$	Grid inductance	2.31 mH	0.5
$R_g$	Grid resistance	$0.29 \Omega$	0.02
$L_f$	Filter inductance	4.62 mH	0.1
$C_f$	Filter capacitance	$32.88 \mu\text{F}$	0.15
$R_f$	Filter resistance	$0.0726 \text{ m}\Omega$	0.005
$J$	Virtual Inertia	$4 S_{ref}/\omega_0$	4
$D_p$	Damping gain	$40 S_{ref}/\omega_0$	40
$D_q$	Q-V Droop gain	$0.1 V_{base}/S_{ref}$	0.1

a)  $R_v = 0.01$  p. u. and voltage sag to  $V_g = 0.6$  p. u.

When the VR is at 0.01 p.u., as shown in Fig. 10, with the occurrence of the voltage sag to 0.6 p.u. of the nominal grid voltage, the system remains stable. In as much as the voltage sag affects the transferred power, according to the definition of the Type 1 transient scenario, both the conventional VSG and the proposed method retain stability owing to the convergence of the system to the existing equilibrium points in the angle dynamics. Therefore, this scenario shows the ideal situation in which the conventional method and the proposed method have identical behaviour.

b)  $R_v = 0.05$  p. u. and voltage sag to  $V_g = 0.6$  p. u.

When  $R_v$  is increased to 0.05 p.u., the conventional method in Fig. 11(a) loses synchronism upon a voltage sag to 0.6 p.u. owing to the effect of VR on the  $P_e$  characteristics. On the other hand, in Fig. 11(b), the proposed method maintains synchronism with the system which shows a damping effect that reduces the angle overshoot and enhances the transient synchronisation stability.

c)  $R_v = 0.05$  p. u. and voltage sag to  $V_g = 0.5$  p. u.

In Fig. 12, the voltage sag is adjusted to 0.5 p.u. As shown by the waveforms, the conventional method loses synchronism almost immediately upon the occurrence of the fault in Fig. 12(a), while the proposed method in Fig. 12(b) has a considerable time lag before there is a loss of synchronism. This reveals superior angle dynamics of the proposed method compared to the conventional VSG and is an indicator of increased critical clearing angle. Therefore, the proposed method is shown to outperform the conventional method by an increased critical clearing time.

d)  $R_v = 0.1$  p. u. and voltage sag to  $V_g = 0.6$  p. u.

When  $R_v$  is increased from 0.05 p.u. to 0.1 p.u., the dynamics of the conventional VSG are further exacerbated as shown in Fig. 13(a) while the proposed method flourishes, owing to the increased damping that is associated with increased  $R_v$  as shown in Fig. 13(b). Compared to Section 5 b), the conventional method loses synchronism in less time with  $R_v = 0.1$  p.u. compared to  $R_v = 0.05$  p.u. On the other hand, the proposed method remains much more stable, which is congruent with the analysis of increased damping using the proposed method.

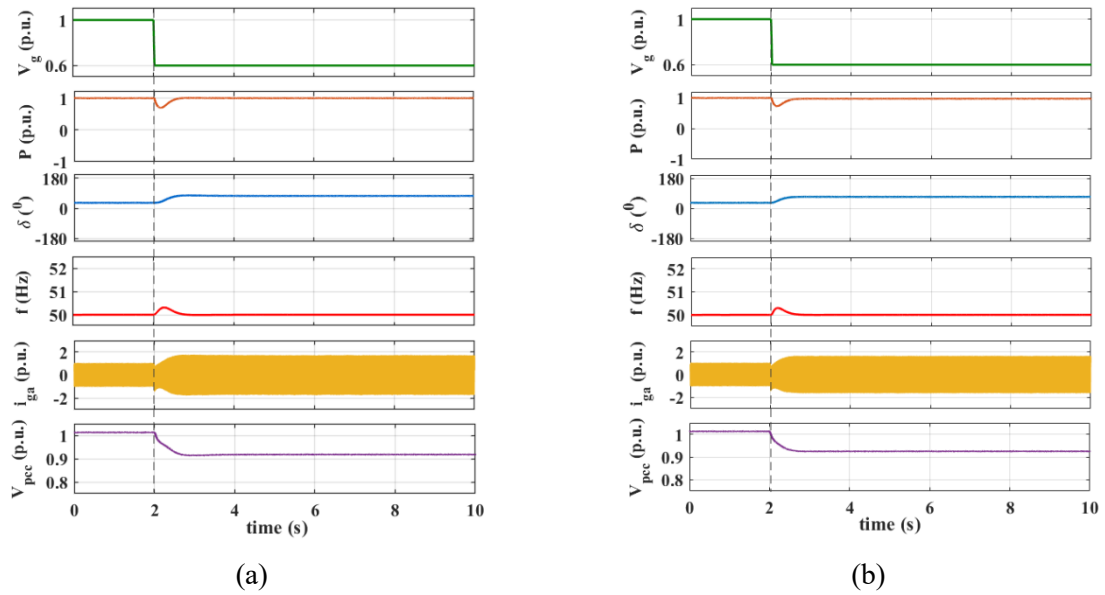


**Fig. 10.** The performance of the VSG with parameters  $R_v = 0.01$  p. u. and voltage sag to  $V_g = 0.6$  p. u. The fault is set to occur at time = 2 seconds indicated by the dotted line. (a) Conventional VSG, (b) proposed method.

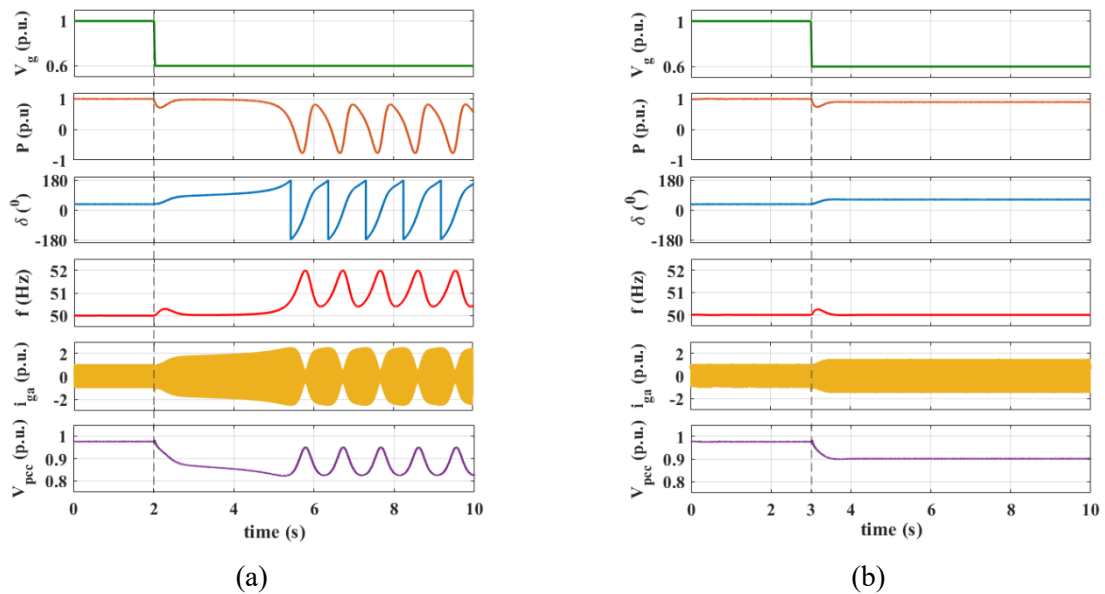


**Fig. 11.** The performance of the VSG with parameters  $R_v = 0.05$  p. u. and voltage sag to  $V_g = 0.6$  p. u. The fault is triggered for the conventional method at time = 2 seconds while for the proposed method at time = 3 seconds. (a) Conventional VSG, (b) proposed method.

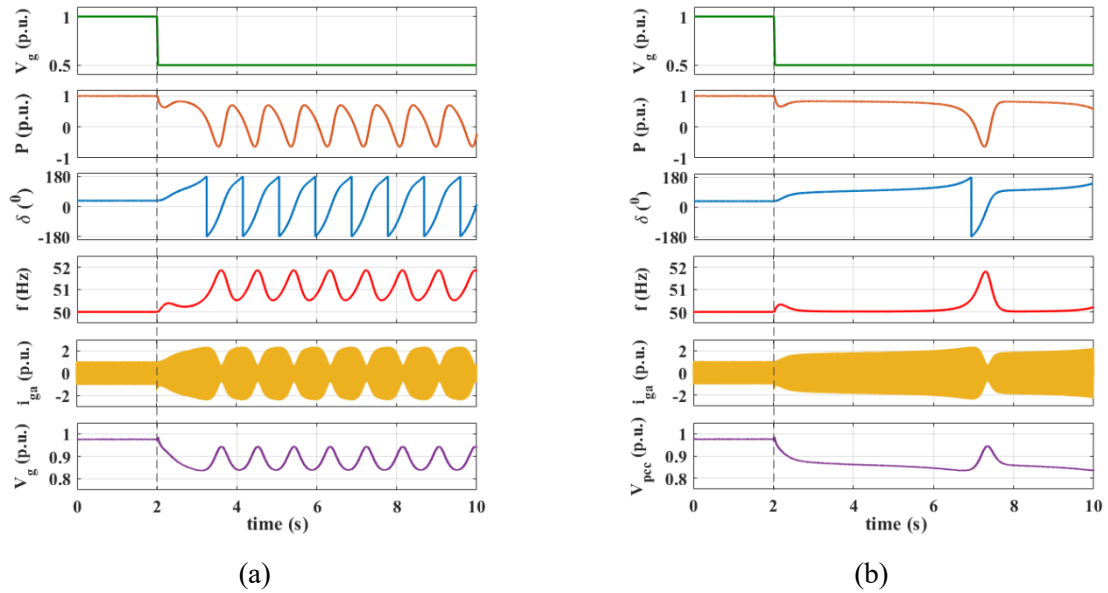


**Fig. 12.** The performance of the VSG with parameters  $R_v = 0.05$  p. u. and voltage sag to  $V_g = 0.5$  p. u. The fault is triggered at time = 2 seconds. (a) Conventional VSG. Loss of synchronism is observed almost immediately upon fault occurrence, (b) proposed method. There is a considerable time lag before the system dynamics are unstable.

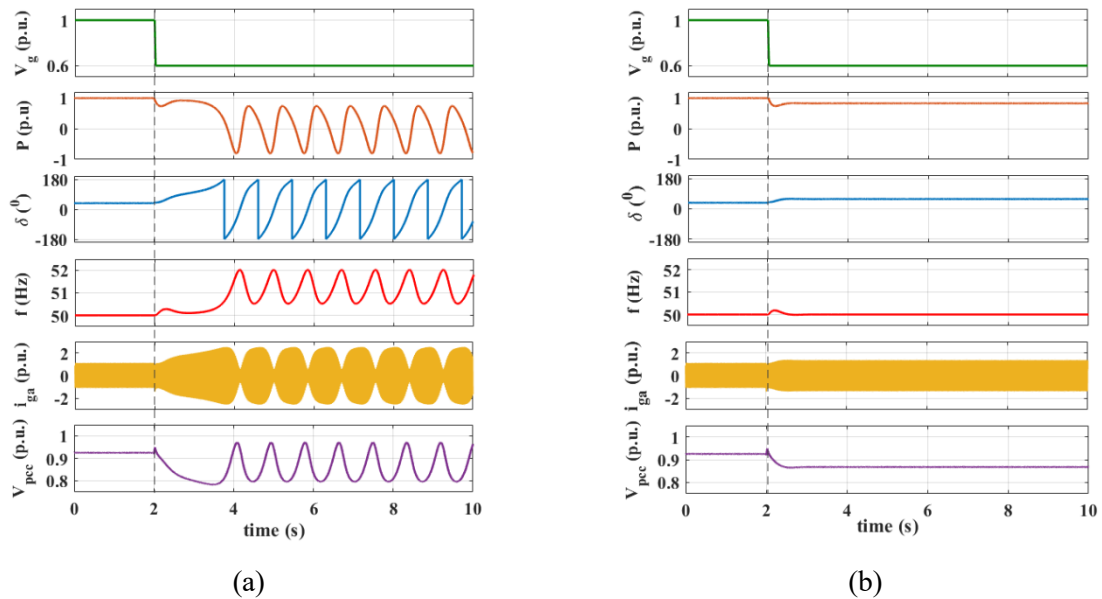


**Fig. 13.** The performance of the VSG with parameters  $R_v = 0.1$  p. u. and voltage sag to  $V_g = 0.6$  p. u. The fault is triggered at time = 2 seconds. (a) Conventional VSG, loss of synchronism is observed, (b) proposed method. The system remains stable.

**6 Conclusion**

This article focuses on the use of VR in damping oscillations in VSG. Using the concept of virtual point of common coupling, it is shown that the use of VR affects the angle stability of VSG in transient synchronisation. A method based on virtual power feed-

back is proposed and shown to be equivalent to a damping term which is a function of the VR and the voltages of the PCC and the grid. Using the proposed method, an enhanced transient performance of VSG is achieved, with verification using simulations in MATLAB/Simulink.

## Acknowledgement

This work was supported by TICAD-7 scholarship under the Egypt Japan University of Science and Technology (EJUST) and the Japan International Cooperation Agency (JICA).

## References

- [1] F. Milano, F. Dorfler, G. Hug, D. J. Hill, and G. Verbie, 'Foundations and Challenges of Low-Inertia Systems (Invited Paper)', in *2018 Power Systems Computation Conference (PSCC)*, Dublin: IEEE, Jun. 2018, pp. 1–25. doi: 10.23919/PSCC.2018.8450880.
- [2] S. Harasis, K. Mahmoud, S. Albatran, K. Alzaareer and Q. Salem, "Dynamic Performance Evaluation of Inverter Feeding a Weak Grid Considering Variable System Parameters," in *IEEE Access*, vol. 9, pp. 126104-126116, 2021, doi: 10.1109/ACCESS.2021.3111047.
- [3] E. Ebinyu, O. Abdel-Rahim, D. A. Mansour, M. Shoyama, and S. M. Abdelkader, 'Grid-Forming Control: Advancements towards 100% Inverter-Based Grids – A Review', *Energies*, vol. 16, no. 22, p. 7579, Nov. 2023, doi: 10.3390/en16227579.
- [4] J. Chen and T. O'Donnell, 'Parameter Constraints for Virtual Synchronous Generator Considering Stability', *IEEE Trans. Power Syst.*, vol. 34, no. 3, pp. 2479–2481, May 2019, doi: 10.1109/TPWRS.2019.2896853.
- [5] S. Chen, Y. Sun, X. Hou, H. Han, S. Fu, and M. Su, 'Quantitative Parameters Design of VSG Oriented to Transient Synchronization Stability', *IEEE Trans. Power Syst.*, vol. 38, no. 5, pp. 4978–4981, Sep. 2023, doi: 10.1109/TPWRS.2023.3293016.
- [6] R. Rosso, X. Wang, M. Liserre, X. Lu, and S. Engelken, 'Grid-Forming Converters: Control Approaches, Grid-Synchronization, and Future Trends – A Review', *IEEE Open J. Ind. Appl.*, vol. 2, pp. 93–109, 2021, doi: 10.1109/OJIA.2021.3074028.
- [7] H. Wu *et al.*, 'Small-Signal Modeling and Parameters Design for Virtual Synchronous Generators', *IEEE Trans. Ind. Electron.*, vol. 63, no. 7, pp. 4292–4303, Jul. 2016, doi: 10.1109/TIE.2016.2543181.
- [8] M. Chen, D. Zhou, C. Wu, and F. Blaabjerg, 'Characteristics of Parallel Inverters Applying Virtual Synchronous Generator Control', *IEEE Trans. Smart Grid*, vol. 12, no. 6, pp. 4690–4701, Nov. 2021, doi: 10.1109/TSG.2021.3102994.
- [9] A. Sajadi, R. W. Kenyon, and B.-M. Hodge, 'Synchronization in electric power networks with inherent heterogeneity up to 100% inverter-based renewable generation', *Nat. Commun.*, vol. 13, no. 1, p. 2490, May 2022, doi: 10.1038/s41467-022-30164-3.
- [10] Y. Li, Y. Gu, Y. Zhu, A. Junyent-Ferre, X. Xiang, and T. C. Green, 'Impedance Circuit Model of Grid-Forming Inverter: Visualizing Control Algorithms as Circuit Elements', *IEEE Trans. Power Electron.*, vol. 36, no. 3, pp. 3377–3395, Mar. 2021, doi: 10.1109/TPEL.2020.3015158.
- [11] J. He and Y. W. Li, 'Analysis, Design, and Implementation of Virtual Impedance for Power Electronics Interfaced Distributed Generation', *IEEE Trans. Ind. Appl.*, vol. 47, no. 6, pp. 2525–2538, Nov. 2011, doi: 10.1109/TIA.2011.2168592.
- [12] J. Rocabert, A. Luna, F. Blaabjerg, and P. Rodríguez, 'Control of Power Converters in AC Microgrids', *IEEE Trans. Power Electron.*, vol. 27, no. 11, pp. 4734–4749, Nov. 2012, doi: 10.1109/TPEL.2012.2199334.
- [13] X. Lu, J. Wang, J. M. Guerrero, and D. Zhao, 'Virtual-Impedance-Based Fault Current Limiters for Inverter Dominated AC Microgrids', *IEEE Trans. Smart Grid*, vol. 9, no. 3, pp. 1599–1612, May 2018, doi: 10.1109/TSG.2016.2594811.
- [14] T. Qoria, F. Gruson, F. Colas, G. Denis, T. Prevost, and X. Guillaud, 'Critical Clearing Time Determination and Enhancement of Grid-Forming Converters Embedding Virtual Impedance as Current Limitation Algorithm', *IEEE J. Emerg. Sel. Top. Power Electron.*, vol. 8, no. 2, pp. 1050–1061, Jun. 2020, doi: 10.1109/JESTPE.2019.2959085.
- [15] Yun Wei Li, 'Control and Resonance Damping of Voltage-Source and Current-Source Converters With LCL Filters', *IEEE Trans. Ind. Electron.*, vol. 56, no. 5, pp. 1511–1521, May 2009, doi: 10.1109/TIE.2008.2009562.
- [16] J. Wang, Y. Wang, Y. Gu, W. Li, and X. He, 'Synchronous frequency resonance of virtual synchronous generators and damping control', in *2015 9th International Conference on Power Electronics and ECCE Asia (ICPE-ECCE Asia)*, Seoul, South Korea: IEEE, Jun. 2015, pp. 1011–1016. doi: 10.1109/ICPE.2015.7167905.
- [17] D. Yang, H. Wu, X. Wang, and F. Blaabjerg, 'Suppression of synchronous resonance for VSGs', *J. Eng.*, vol. 2017, no. 13, pp. 2574–2579, Jan. 2017, doi: 10.1049/joe.2017.0792.
- [18] T. Qoria, 'Grid-forming control to achieve a 100% power electronics interfaced power transmission systems', PhD Thesis, HESAM University, 2020.
- [19] S. Fu, Y. Sun, L. Li, Z. Liu, H. Han and M. Su, "Power Oscillation Suppression in Multi-VSG Grid by Adaptive Virtual Impedance Control," in *IEEE Systems Journal*, vol. 16, no. 3, pp. 4744-4755, Sept. 2022, doi: 10.1109/JSYST.2022.3173666.
- [20] L. Harnefors, M. Hinkkanen, U. Riaz, F. M. M. Rahman, and L. Zhang, 'Robust Analytic Design of Power-Synchronization Control', *IEEE Trans. Ind. Electron.*, vol. 66, no. 8, pp. 5810–5819, Aug. 2019, doi: 10.1109/TIE.2018.2874584.
- [21] M. G. Taul, X. Wang, P. Davari, and F. Blaabjerg, 'Current Limiting Control With Enhanced Dynamics of Grid-Forming Converters During Fault Conditions', *IEEE J. Emerg. Sel. Top. Power Electron.*, vol. 8, no. 2, pp. 1062–1073, Jun. 2020, doi: 10.1109/JESTPE.2019.2931477
- [22] S. P. Me, S. Zabihi, F. Blaabjerg, and B. Bahrani, 'Adaptive Virtual Resistance for Postfault Oscillation Damping in Grid-Forming Inverters', *IEEE Trans. Power Electron.*, vol. 37, no. 4, pp. 3813–3824, Apr. 2022, doi: 10.1109/TPEL.2021.3118677.
- [23] X. Xiong, C. Wu, and F. Blaabjerg, 'Effects of Virtual Resistance on Transient Stability of Virtual Synchronous Generators Under Grid Voltage Sag', *IEEE Trans. Ind. Electron.*, vol. 69, no. 5, pp. 4754–4764, May 2022, doi: 10.1109/TIE.2021.3082055.
- [24] H. Wu and X. Wang, 'A Mode-Adaptive Power-Angle Control Method for Transient Stability Enhancement of Virtual Synchronous Generators', *IEEE J. Emerg. Sel. Top. Power Electron.*, vol. 8, no. 2, pp. 1034–1049, Jun. 2020, doi: 10.1109/JESTPE.2020.2976791.
- [25] R. Sun, J. Ma, W. Yang, S. Wang, and T. Liu, 'Transient Synchronization Stability Control for LVRT With Power Angle Estimation', *IEEE Trans. Power Electron.*, vol. 36, no. 10, pp. 10981–10985, Oct. 2021, doi: 10.1109/TPEL.2021.3070380.
- [26] X. Xiong, C. Wu, B. Hu, D. Pan, and F. Blaabjerg, 'Transient Damping Method for Improving the Synchronization Stability of Virtual Synchronous Generators', *IEEE Trans. Power Electron.*, vol. 36, no. 7, pp. 7820–7831, Jul. 2021, doi: 10.1109/TPEL.2020.3046462.
- [27] D. Pan, X. Wang, F. Liu, and R. Shi, 'Transient Stability of Voltage-Source Converters With Grid-Forming Control: A Design-Oriented Study', *IEEE J. Emerg. Sel. Top. Power Electron.*, vol. 8, no. 2, pp. 1019–1033, Jun. 2020, doi: 10.1109/JESTPE.2019.2946310.

- [28] M. Chen, D. Zhou, and F. Blaabjerg, 'Enhanced Transient Angle Stability Control of Grid-Forming Converter Based on Virtual Synchronous Generator', *IEEE Trans. Ind. Electron.*, vol. 69, no. 9, pp. 9133–9144, Sep. 2022, doi: 10.1109/TIE.2021.3114723.
- [29] X. Xiong, C. Wu, and F. Blaabjerg, 'An Improved Synchronization Stability Method of Virtual Synchronous Generators Based on Frequency Feedforward on Reactive Power Control Loop', *IEEE Trans. Power Electron.*, vol. 36, no. 8, pp. 9136–9148, Aug. 2021, doi: 10.1109/TPEL.2021.3052350.
- [30] S. Chen, Y. Sun, H. Han, S. Fu, S. Luo, and G. Shi, 'A Modified VSG Control Scheme With Virtual Resistance to Enhance Both Small-Signal Stability and Transient Synchronization Stability', *IEEE Trans. Power Electron.*, vol. 38, no. 5, pp. 6005–6014, May 2023, doi: 10.1109/TPEL.2023.3243025.
- [31] J. Fang, W. Si, L. Xing, and S. M. Goetz, 'Analysis and Improvement of Transient Voltage Stability for Grid-Forming Converters', *IEEE Trans. Ind. Electron.*, vol. 71, no. 7, pp. 7230–7240, Jul. 2024, doi: 10.1109/TIE.2023.3299023.
- [32] N. Alamir, O. Abdel-Rahim, M. Ismeil, M. Orabi and R. Kennel, "Fixed Frequency Predictive MPPT for Phase-Shift Modulated LLC Resonant Micro-Inverter," 2018 20th European Conference on Power Electronics and Applications (EPE'18 ECCE Europe), Riga, Latvia, 2018, pp. P.1-P.9.
- [33] O. Abdel-Rahim and H. Furiato, "Switched inductor quadratic boosting ratio inverter with proportional resonant controller for grid-tie PV applications," IECON 2014 - 40th Annual Conference of the IEEE Industrial Electronics Society, Dallas, TX, USA, 2014, pp. 5606-5611, doi: 10.1109/IECON.2014.7049358.
- [34] O. Abdel-Rahim, H. Funato and J. Haruna, "An efficient MPPT technique with fixed frequency finite-set model predictive control," 2015 IEEE Energy Conversion Congress and Exposition (ECCE), Montreal, QC, Canada, 2015, pp. 6444-6449, doi: 10.1109/ECCE.2015.7310562.
- [35] O. Abdel-Rahim, N. Alamir, M. Orabi, et al., "Fixed-frequency phase-shift modulated PV-MPPT for LLC resonant converters," *J. Power Electron.* 20, 279–291 (2020). <https://doi.org/10.1007/s43236-019-00001-w>
- [36] M. Chen, D. Zhou, and F. Blaabjerg, 'Voltage Control Impact on Performance of Virtual Synchronous Generator', in *2021 IEEE 12th Energy Conversion Congress & Exposition - Asia (ECCE-Asia)*, Singapore, Singapore: IEEE, May 2021, pp. 1981–1986. doi: 10.1109/ECCE-Asia49820.2021.9479084.
- [37] X. Li, Y. Hu, Y. Shao, and G. Chen, 'Mechanism analysis and suppression strategies of power oscillation for virtual synchronous generator', in *IECON 2017 - 43rd Annual Conference of the IEEE Industrial Electronics Society*, Beijing: IEEE, Oct. 2017, pp. 4955–4960. doi: 10.1109/IECON.2017.8216855.
- [38] P. Kundur, N. J. Balu, and M. G. Lauby, *Power system stability and control*. in The EPRI power system engineering series. New York San Francisco Washington [etc.]: McGraw-Hill, 1994.
- [39] I. Sadeghkhani, M. E. Hamedani Golshan, A. Mehrizi-Sani, J. M. Guerrero, and A. Ketabi, 'Transient Monitoring Function-Based Fault Detection for Inverter-Interfaced Microgrids', *IEEE Trans. Smart Grid*, pp. 1–1, 2016, doi: 10.1109/TSG.2016.2606519.
- [40] 'IEEE Standard for Interconnection and Interoperability of Distributed Energy Resources with Associated Electric Power Systems Interfaces'. IEEE. doi: 10.1109/IEEESTD.2018.8332112.
- [41] Z. Shuai, C. Shen, X. Liu, Z. Li, and Z. J. Shen, 'Transient Angle Stability of Virtual Synchronous Generators Using Lyapunov's Direct Method', *IEEE Trans. Smart Grid*, vol. 10, no. 4, pp. 4648–4661, Jul. 2019, doi: 10.1109/TSG.2018.2866122

Received 7 July 2024

---